Molecular Electronics Hot Paper

International Edition: DOI: 10.1002/anie.201906032
German Edition: DOI: 10.1002/ange.201906032

A Solid-State Protein Junction Serves as a Bias-Induced Current Switch

Jerry A. Fereiro, Ben Kayser, Carlos Romero-Muñiz, Ayelet Vilan, Dmitry A. Dolgikh, Rita V. Chertkova, Juan Carlos Cuevas, Linda A. Zotti,* Israel Pecht,* Mordechai Sheves,* and David Cahen**

Abstract: *A sample-type protein monolayer, that can be a stepping stone to practical devices, can behave as an electrically driven switch. This feat is achieved using a redox protein, cytochrome C (CytC), with its heme shielded from direct contact with the solid-state electrodes. Ab initio DFT calculations, carried out on the CytC–Au structure, show that the coupling of the heme, the origin of the protein frontier orbitals, to the electrodes is sufficiently weak to prevent Fermi level pinning. Thus, external bias can bring these orbitals in and out of resonance with the electrode. Using a cytochrome C mutant for direct S–Au bonding, approximately 80 % of the Au–CytC–Au junctions show at greater than 0.5 V bias a clear conductance peak, consistent with resonant tunneling. The on–off change persists up to room temperature, demonstrating reversible, bias-controlled switching of a protein ensemble, which, with its built-in redundancy, provides a realistic path to protein-based bioelectronics.*

Introduction

Protein-based electrical junctions, exhibiting non-linear current–voltage characteristics, may provide a route to future bioelectronic applications.[1,2] The ability to rationally design protein-based electrical components, requires fundamental understanding of their charge-transport mechanism.[1,3,4] Earlier studies have shown that the characteristics of electronic charge transport, ETp, via protein junctions are influenced by the protein structure,[5–7] electrode–protein coupling,[8–10] and the alignment of frontier molecular orbital energies with respect to the Fermi levels (E_F) of the electrode,[11,12] often characterized by a single parameter known as the energy barrier.[13]

The combination of protein molecular orbitals and their coupling to the electrodes dictates the transmission probability across the junction. A large variation of the transmission as a function of electron energy (determined by bias voltage across the junction) yields a highly non-linear current–voltage response. A situation where the applied bias window aligns with the Fermi level of one of the electrodes is known as resonant and is identified by a peak in the conductance–voltage response. While conductance resonances were often observed in scanning tunneling microscopy (STM) measurements,[14–16] they are rather rare with two intimate contacts. A possible reason is that in an intimate contact junction, where the electronic states of the molecules at both ends are coupled to those of the electrode, partial charge transfer can occur between the electrode and molecules until an equilibrium is achieved.[13] This interaction between molecular and electrode electronic states influences the energy level alignment of the frontier orbital energy levels in the molecules.[8] Normally stronger interaction pushes the energy levels further away in energy from the equilibrium Fermi level.[11] In most cases, the molecular junctions are so delicate that electrical break down happens before the bias voltage, required for resonance, is reached. Here, for intimate contact junctions, the entire system i.e., the molecules along with the electrodes must be taken into account for understanding the energy-level alignment of the frontier orbitals.[13]

If no peaks are observed, it is often assumed that the non-linear part of the current–voltage response reflects the "shoulders" of a resonance, without actually reaching it.[17] We showed previously that inserting a linker molecule between the electrode and the protein[9] can weaken the coupling strength between them, and the ETp mechanism can be switched from resonant to off-resonant tunneling by chemically modulating this strength.[11] Since this is a chemically modulated process, two sets of samples with different junction configurations (one with and one without the linker) are needed to achieve this, meaning that in a single working junction we either have resonant or off-resonant tunneling transport. Herein, we report a clear observation of conductance resonances in an intimate contact protein junction (without any linker) by only varying the applied bias. The major step here over the previously reported result is that the

[*] Dr. J. A. Fereiro, Dr. B. Kayser, Dr. A. Vilan, Prof. D. Cahen
Department of Materials and Interfaces,
Weizmann Institute of Science, Rehovot (Israel)
E-mail: ayelet.vilan@weizmann.ac.il
david.cahen@weizmann.ac.il
Prof. D. A. Dolgikh, Prof. R. V. Chertkova
Shemyakin-Ovchinnikov Institute of Bioorganic Chemistry,
Russian Academy of Science, Moscow (Russia)
Dr. C. Romero-Muñiz, Prof. J. C. Cuevas, Prof. L. A. Zotti
Departamento de Física Teórica de la Materia Condensada and
Condensed Matter Physics Center (IFIMAC),
Universidad Autónoma de Madrid, 28049 Madrid (Spain)
E-mail: linda.zotti@uam.es
Prof. I. Pecht
Department of Immunology, Weizmann Institute of Science
Rehovot (Israel)
E-mail: Israel.pecht@weizmann.ac.il
Prof. M. Sheves
Department of Organic Chemistry, Weizmann Institute of Science
Rehovot (Israel)
E-mail: mudi.sheves@weizmann.ac.il
Supporting information and the ORCID identification number(s) for the author(s) of this article can be found under: https://doi.org/10.1002/anie.201906032.

transition from off- to on- resonance is achieved within the same working junction.

C-type cytochromes (CytC) constitute a family of redox-active proteins that act as electron carriers in biological energy-conversion systems.[18] Their redox activity arises from the presence of a heme group (Fe, coordinated by protoporphyrin IX) mediating electrons between their heme Fe^{II}/hemin Fe^{III} states.[18] Herein, we present the observation of a transition from off- to on-resonant tunneling at moderate bias (less than 1 V) in the conductance via a CytC covalently attached to a gold (Au) substrate by a thiol residue (mutated cysteine 104, E104C). The low voltage (less than 0.5 V) conductance–voltage characteristics are consistent with an off-resonant tunneling process, as also supported by clear inelastic electron tunneling spectroscopy (IETS) features. At higher voltages (greater than 0.5 V), an abrupt increase in conductance up to one order of magnitude is observed, followed by a slight decrease. We interpret this conductance peak as direct evidence for resonant tunneling and propose that the heme/hemin cofactor energy levels of the CytC(E104C) are involved in the charge transport process.

To investigate the role of heme/hemin energy levels in this unique charge transport behavior, we carried out ab initio calculations, using density functional theory, on the whole structure of the CytC(E104C) mutant attached to a Au surface, as well as in its free gas-phase state. The projected density of states (PDOS) for some relevant atoms reveal that the levels closest to the Fermi level originate from the hemin's Fe^{III} center and porphyrin. These frontier orbitals are assumed to dominate the electron transport, and indeed their computed energy position fits well with the conductance resonances. Our results suggest a bias dependent off- to on-resonant charge-transport transition via a protein-based solid-state junction. This method permits us to understand the energy-level alignment involved in complex electrode–protein systems. Understanding the factors that promote the emergence of conductance resonance, within accessible bias values, will help us to design biologically inspired bioelectronic devices with new functions, not possible with conventional semiconductor devices.

Results and Discussion

Figure 1 A shows schematically the structure of the Au–CytC(E104C)–Au nanowire (NW) junction configuration employed in this study. Current–voltage (I–V), conductance–voltage (dI/dV–V), and d^2I/dV^2–V (IETS) data were obtained simultaneously, using direct source-meter measurements and a lock-in amplifier. Low temperature I–V measurements of CytC(E104C) monolayers show two distinct conductance regimes corresponding to different ranges of the applied source-to-drain voltages: 1) region I measured at bias (less than 0.5 V), where a linear current response to applied voltage was observed (shaded with sky blue color in Figure 1 B), and 2) region II at bias (greater than 0.5 V), with a strong non-linear current response (yellow shading in Figure 1 B). The changes in the I–V curve corresponding to different applied potential ranges become more obvious if we look at the black line in Figure 1 B, which shows the differential conductance vs. applied voltage. Up to 0.5 V (region I) a relatively constant conductance value is observed, which increases by up to 10-fold in region II. We attribute the different maximal conductance values at positive and negative biases to unequal voltage drops at the two protein–Au interfaces.

Figure 1 C shows the zoomed-in plot of region I in Figure 1 B. The small kinks observed in the dI/dV–V plot in region I, (Figure 1 C-black line), are consistent with the opening of inelastic conduction channels at voltages corresponding to energies of vibrational modes, while the dip near zero bias is attributed to the large number of low-energy vibrations. The observed peak in the IETS spectrum (d^2I/dV^2–V) in region I (Figure 1 E) around 0.37 V (3000 cm^{-1}) corresponds to the C–H stretching mode and those at 0.20/0.18 V (1640/1520 cm^{-1}) correspond to the amide I and amide II bands, respectively.[20] As we have reported earlier, the small kinks observed in the dI/dV–V plot (less than 0.5 V, Figure 1 C), which translate into the peaks observed in the IETS spectra (Figure 1 E), are typical for off-resonance transport through the protein junction.[9]

Conductance Resonances

A simple way to rationalize the observed conductance peaks is by assuming that the electron transport is coherent and by approximating the transmission function as a single Lorentzian shaped peak, centred at ε eV above or below the Fermi energy. Using Landauer formalism, this yields the following conductance (G)–voltage relation,[23–25] a low temperature formula valid when gamma (Γ) $\gg k_B T$:

$$G = NG_0\Gamma^2\left\{\frac{0.5-\alpha}{[(1-2\alpha)V-2\varepsilon]^2+\Gamma^2}+\frac{0.5+\alpha}{[(1+2\alpha)V+2\varepsilon]^2+\Gamma^2}\right\} \quad (1)$$

Here Γ is the coupling energy (in eV, assuming the same coupling to each contact, for simplicity) or the width of the Lorentzian peak and α (dimensionless) measures the voltage partition between the two contacts. In the symmetric case, the voltage is divided evenly between the two contacts and $\alpha \equiv 0$; the opposite extreme is if the entire voltage drops over only on one contact and $\alpha = \pm 0.5$ ($|\alpha| \leq 0.5$); N is the number of molecules in parallel and $G_0 = 2\frac{e^2}{h}$ is the quantum of conductance.

In principle, the center of the conductance peaks occurs at $V_{max}^{+,-} = \pm 2\varepsilon/(1 \mp 2\alpha)$. Since most junctions are rather symmetric ($\alpha \approx 0$), we identify the peak centre with twice the energy offset of the dominant transport level from the Fermi level. For example, in Figure 2, the two peaks are located at $+0.95$ and -0.76 V, which translates into $\varepsilon = 0.48$ eV (blue line) and $\varepsilon = 0.38$ eV (red line), if each peak is fitted separately, or to $\varepsilon = 0.45$ eV when we use one fit to capture the entire voltage range (green line). However, the energy offset can also be derived directly from the peak positions: $\varepsilon = |V_{max}^{+}V_{max}^{-}|/(|V_{max}^{+}| + |V_{max}^{-}|)$. One of the most important attributes of this procedure is that the peak is a measurable

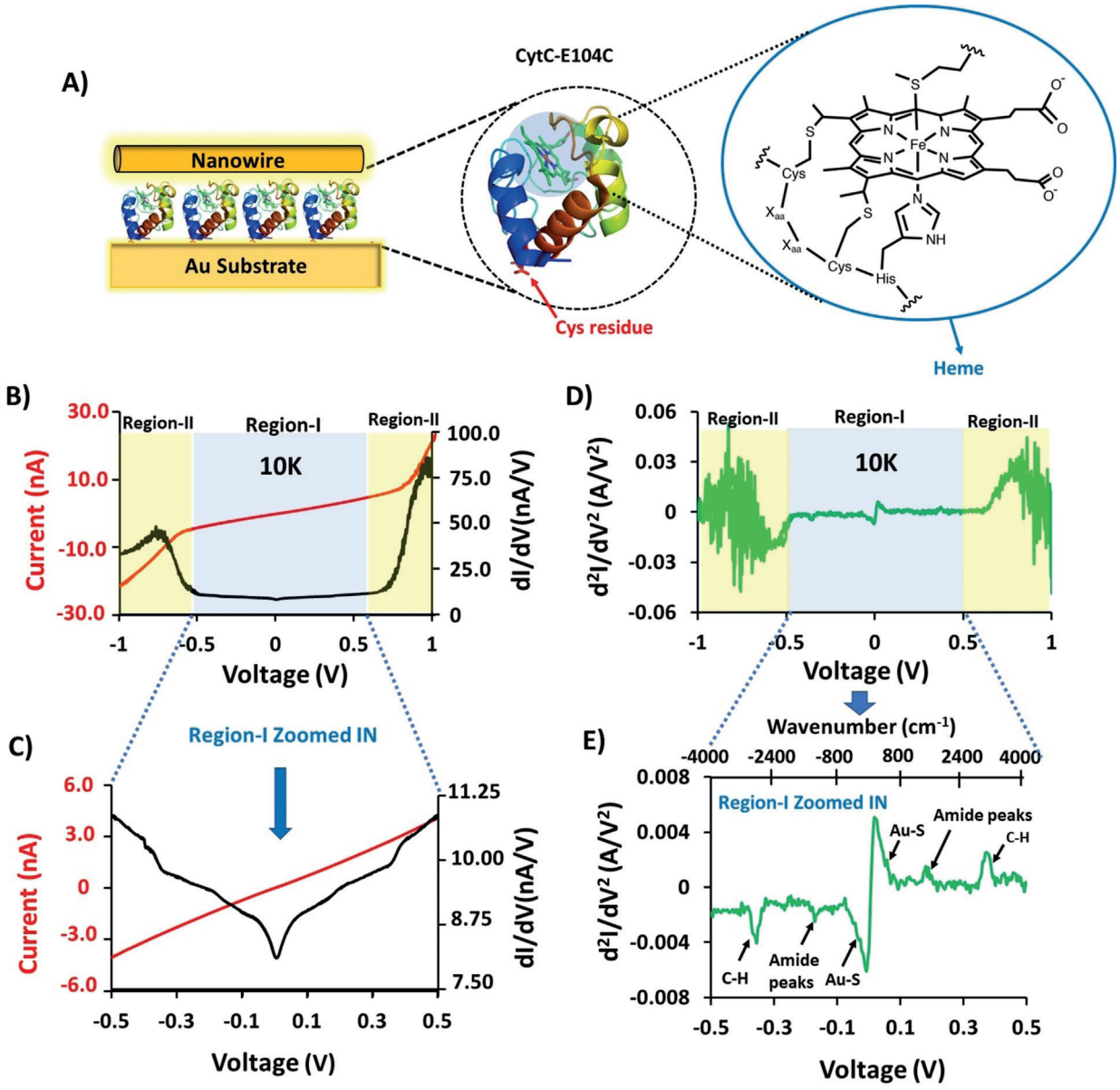

Figure 1. A) Schematic illustration of the solid-state protein junction prepared by trapping the nanowires to produce contacts for electrical transport measurements. The inset shows the 3D structure of Cyt C (PDB: 1HRC), where red sticks denote the thiolate residue used for binding to the Au substrate. The inner part shows the heme center (enlarged in the right-most inset). B) Current–voltage, *I*–*V* (red, left-axis) and conductance–voltage, d*I*/d*V*–*V* (black, right-axis) plots of the Au–CytC(E104C)–Au junction; C) Zoom-in of *I*–*V* (red) and d*I*/d*V*–*V* (black) plots of region I between −0.5 and +0.5 V. D) IETS, d^2I/dV^2–*V*, plot of CytC(E104C) between −1.0 and +1.0 V. E) Zoom-in of IETS plot in region I between −0.5 V and +0.5 V.

quantity and therefore does not require any assumptions or fit parameters for its determination.

The fitting of the experimental *G*–*V* data to single level Lorentzians (lines in Figure 2) reveal a rather consistent energy offset of approximately 0.4 eV, except for the low-voltage fit (yellow line) that is considered below. Nevertheless, wide-range fitting, in contrast to threshold values (for example, peak positions) reveal significant deviations from simplified models, which is expected considering that a perfect Lorentzian is a gross over-simplification of the real transmission function. A few experimental aspects cannot be reproduced by Equation (1): the maximal conductance values at positive and negative biases have different heights ($G^{+}_{max} > G^{-}_{max}$) and locations ($|V^{+}_{max}| > |V^{-}_{max}|$), the "too-wide" conductance peaks and the very flat conductance gap (low-voltage range).

The first inconsistency is not obvious because Equation (1) in principle tolerates different peak positions and height by introducing α. It is even possible to recover α from either one of the peak position: $2\alpha_V = (|V^{+}_{mx}| - |V^{-}_{mx}|)/(|V^{+}_{mx}| + |V^{-}_{mx}|)$ or from the maximal conductance values: $2\alpha_G = -(r_{\pm}-1)/(r_{\pm}+1)$, where $r_{\pm} = G^{+}_{max}/G^{-}_{max}$. It implies that the peak that is located closer to 0 V and should also have a higher magnitude, which is not

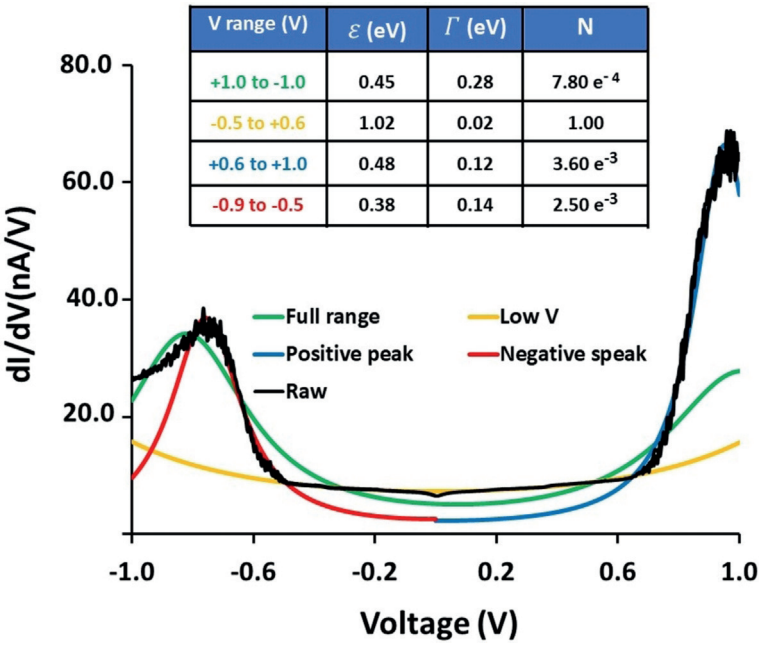

Figure 2. Fitting to a single Lorentzian approximation plotted over the experimentally measured conductance–voltage response. Black line shows raw data and other lines are fits to Equation (1) over different voltage ranges; the fitting parameters are given in the table inset.

so in Figure 2, which yields $\alpha_V = +0.05$ cf. $\alpha_G = -0.14$. The second issue is the width of the conductance peak (Γ), Equation (1) predicts a direct relation between the broadening (denominator) and the net conductance (pre-factor). A broadening of $\Gamma \approx 0.1$ eV (see the Table in Figure 2) implies an about 1000 times larger current than is actually measured. Equation (1) solves this problem by allowing the involvement of an unknown number of molecules, N; however, this is relevant only for $N \geq 1$, which is not the case here. This implies that either there is an additional step that drastically reduces the transmission probability, or that the apparent peak-width does not reflect the real coupling but rather a collection of closely spaced energy levels.

Finally, the experimental G–V trace shows a sharp conductance onset i.e., switching between low and high voltage regimes. This is in contrast to the mild, gradual conductance increase predicted by the Lorentzian model. As an exercise, we fitted Equation (1) to the data obtained in the flat-gap region only (yellow line of Figure 2). This yields an extrapolated resonance, far beyond the actual resonance ($\varepsilon \approx 1$ eV, $\rightarrow V_{mx} \approx 1$ V, see the Table in Figure 2). Such an off-resonance fit is dominated only by ε and therefore Γ can be adjusted to reflect that current magnitude. This yields $\Gamma = 0.02$ eV if the junction contains only a single molecule and a 10–50 fold smaller Γ for a realistic number of molecules conducting in parallel (100–2500, respectively). In summary, the clear conductance resonances give a definite indication of the location of molecular energy levels involved in the transport. At the same time, the observed G–V dependence is beyond a simplistic single-level model, and its details are yet to be explored.

The junction stability and the reproducibility of our measurements were tested by using different samples prepared on different days as well as several junctions within each sample (Supporting Information, Figure S5 A). The resonance energy varies slightly from junction to junction due to the slight change in the orientation of CytC(E104C) on the Au surface (Supporting Information, Figure S6). In total, 25 out of 32 measured junctions that gave stable results showed peaks (Supporting Information, Figure S6). Other remaining junctions showed a gradual rise in conductance with the applied bias, without clear peak-like features (Supporting Information, Figure S7). Therefore, the position of the conductance peaks varied slightly (± 0.15 V) between different junctions. By averaging the peak values obtained from 25 different junctions, we got an effective energy barrier of 0.40 ± 0.08 V (i.e. half the peak value, in volts) for Au–CytC(E104C)–Au junctions.

Computational Studies

To understand the origin of the resonances observed in the dI/dV curves, we performed density functional theory (DFT) calculations on CytC(E104C) bound on a Au surface as well as in its isolated state in the gas phase. For this purpose, we used the OpenMX code,[26,27] which was successfully used in previous studies of proteins of similar size.[28] Further computational details are reported in the Section 7 of the Supporting Information. Figure 3 A (side view) and Figure 3 B (top view) show the structure of the system

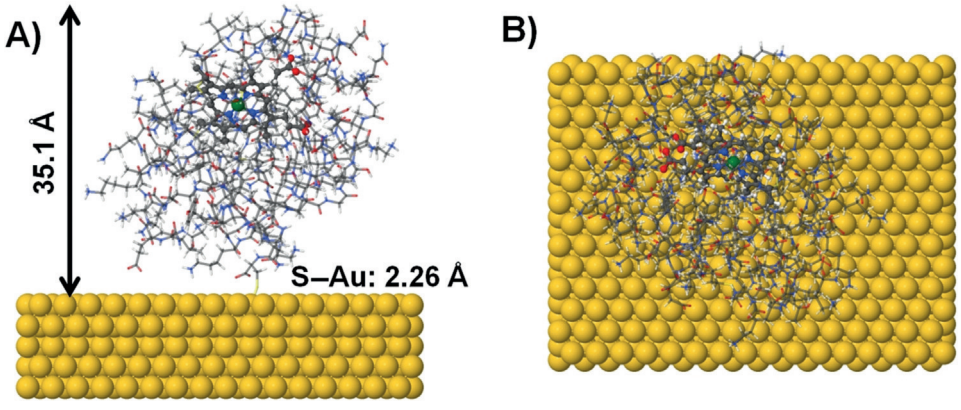

Figure 3. CytC(E104C) mutant adsorbed on a five-layer Au slab in A) side view and B) top view.

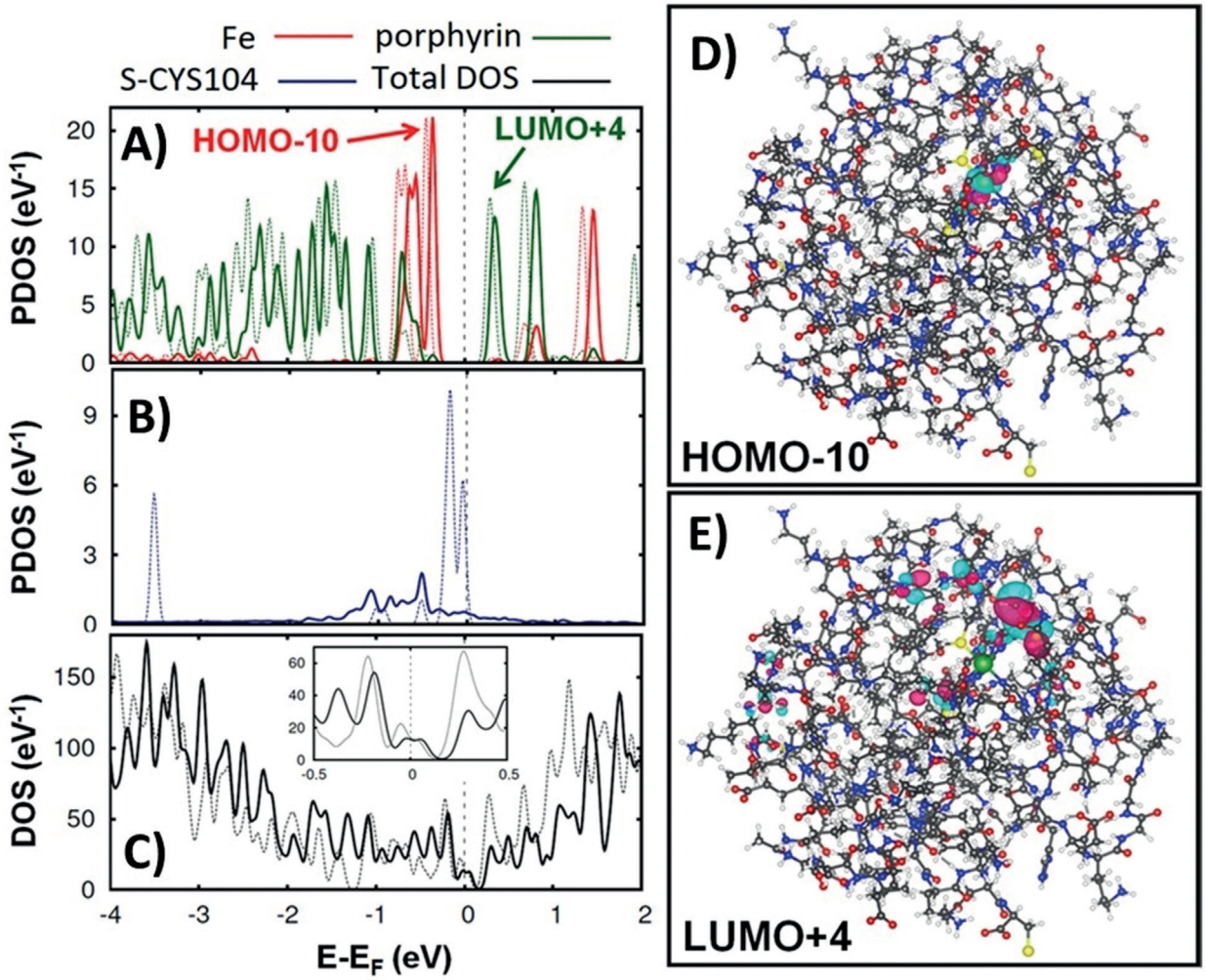

Figure 4. A) Projected density of states (PDOS) on the Fe^{III} ion (red) and on the porphyrin ring (green) B) and on the S atom of the cysteine at position 104; C) total density of states of the whole CytC(E104C); D) spatial distribution of HOMO-10; E) and LUMO + 4. For panels (A)–(C), solid lines correspond to CytC on the five-layer gold surface, whereas the dashed lines correspond to the gas phase. The Fe^{III} ion and the porphyrin are the moieties most likely to play a dominant role in the electron transport.

analyzed, in which CytC is adsorbed on a five-layer Au surface and is oriented so as to bind to the Au surface via the S atom of the cysteine at position 104.

In Figure 4, we present A) the PDOS for the Fe^{III} ion and the porphyrin as well as B) for the S atom of the cysteine at position 104. For each one, a comparison between the behavior in the gas phase (dotted lines) and in the presence of the Au surface (solid lines) is shown, as is also the case for the total density of states, which is displayed in Figure 4C. Figure 4A shows that the PDOS on both the Fe^{III} center and the porphyrin preserve the main features from the gas phase when CytC is adsorbed on Au. This is not surprising as the heme/hemin lies at a considerable distance (around 20 Å) from the surface. Conversely, the PDOS for the S atom of the cysteine at position 104, which is responsible for the protein S–Au bond, is changed drastically upon adsorption onto the surface (Figure 4B), so that the peaks closer to the Fermi level are now broadened, flattened, and shifted downwards in energy. Overall, a charge transfer of approximately seven electrons takes place at the interface from the metal to the protein. As for the total density of states, no remarkable changes overall are observed between the protein in the gas phase and on the Au surface (Figure 4C).

An a priori association of the peaks observed in the PDOS profile of Figure 4A with the resonances observed in the experimental dI/dV curve of Figure 1B is not straightforward. The theoretical curve of the PDOS of the whole protein shows non-negligible contributions over the entire energy range, even around the Fermi energy. A close-up inspection of the spatial distribution of the frontier orbitals of CytC reveals, however, that the bump present in the PDOS at the Fermi energy (Figure 4C inset) most likely originates from localized states on the periphery of the protein, and therefore does not play a major role in the electron transport. Instead, the 1 eV gap observed in the curve of Figure 1B, together with the spatial distribution obtained theoretically for HOMO-10 and LUMO + 4 lead us to identify these two orbitals as possible channels responsible for the current flow. They are localized on the Fe^{III} ion and on the porphyrin, respectively (Figure 4D and E), although LUMO + 4 seems to be more delocalized than HOMO-10.

The ambiguous direction of the conductance asymmetry (α, Figure 2) does not allow us to resolve whether the transport occurs via filled or empty states. Moreover, the LUMO + 4 and HOMO-10 lie at about the same energy from the Fermi level and could consequently both fall in the energy window defined by the voltage. However, the wide broadening of the experimental resonances (approximately 300 mV) suggests the involvement of more than one level, positioned at approximately 0.4 eV from the Fermi level. Therefore, the electron transport through this system could be governed by levels in both the occupied and unoccupied energy range, even including levels below the HOMO-10 and above LUMO + 4. It is worth noting that an involvement of the heme ring was suggested in a previous study.[29] In any case, a complete electron-transport calculation of the junction is needed to clarify this issue, which is beyond the scope of this work as it is computationally too demanding.

Temperature Dependence and Proposed Mechanism

To test the proposed transport mechanism, we examined the temperature dependence of the Au–CytC–Au junctions. Figure 5A shows the conductance–voltage plots corresponding to the current–voltage plots shown in Figure S13A in the Supporting Information, determined at different temperatures ranging from 10 to 120 K. To sharpen the observed conductance plots in Figure 5A, we carried out a normalized differential conductance (dI/dV*V/I)) analysis[30,31] for different temperature ranges (Supporting Information, Figures S8 and S13). The inset plot of Figure 5A shows the evolution of the peak position (energy offset, blue) and peak width (Γ, red) with temperature. These values were extracted by fitting the *G*–*V* data at each temperature to Equation (1); the fit was limited to *G* values larger than one tenth of the maximal conductance value and for positive voltage only (same procedure as used to create the blue-line in Figure 2). The extracted peak-width values (Figure 5A inset), are larger than the thermal energy $k_B T$, pointing to the broadening of the Fermi–Dirac distribution of the contacts. As we showed in detail previously,[11] results from the temperature dependence of the conductance–voltage plots helps to exclude other possibilities, such as Coulomb blockade. Specifically at the Coulomb blockade regime the conductance peak decreases as $1/k_B T$,[25] which is not what is seen for the Au–CytC–Au junctions.

Figure 5B shows a proposed energy level diagram for the scenario where the applied bias is less than 0.5 V. For the sake of clarity, we only focus on the LUMO. When this orbital is located far above the Fermi level, the current is low due to a small off-resonant contribution from the tail of the LUMO. With an increase in applied bias to greater than 0.5 V (Figure 5C), the energy levels align within the bias window, resulting in resonant tunneling with a rather abrupt increase

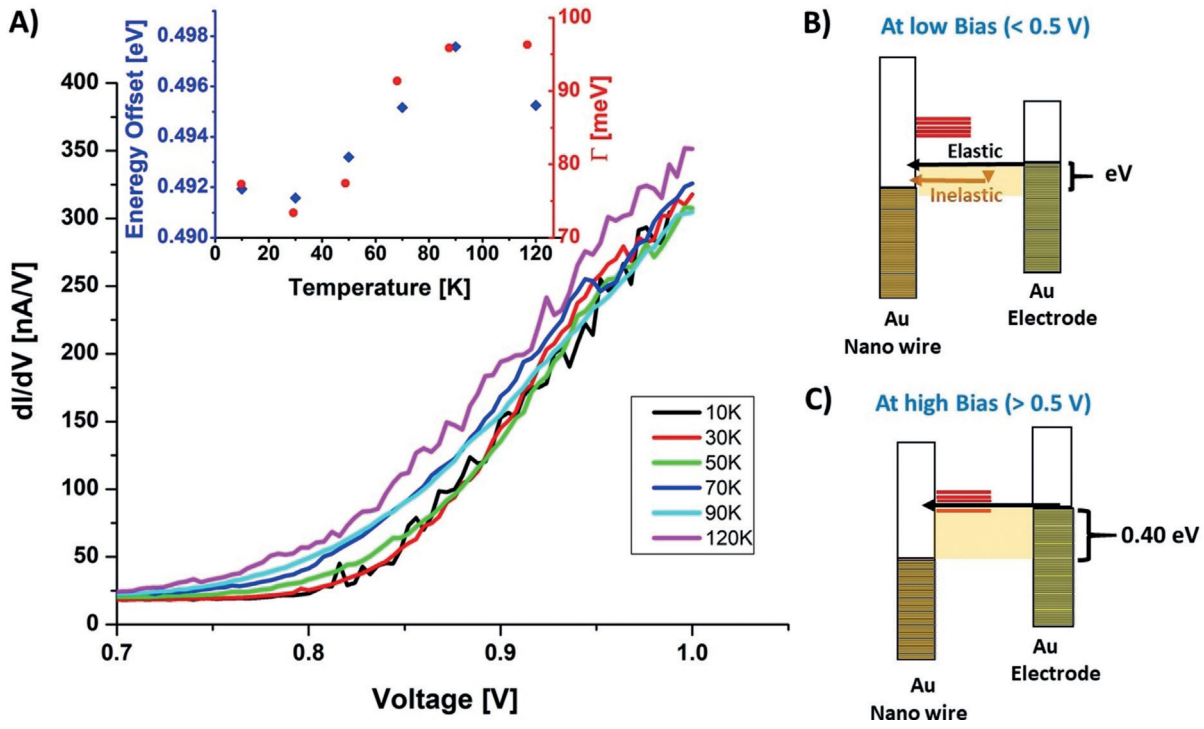

Figure 5. A) Conductance–voltage plots corresponding to the current–voltage plots (Supporting Information, Figure S13A) for different temperatures ranging from 10 K to 120 K, in the positive bias range. The inset plot of Figure 5A shows the evolution of the peak position (energy offset, blue) and peak width (Γ, red) with temperature. B) Schematic illustration of a solid-state protein junction, indicating off-resonant tunneling (bias less than 0.5 V in our experiments). The black arrow indicates elastic tunneling and the orange arrow shows an inelastic tunneling process. C) as (B), but for resonant tunneling (bias greater than 0.5 V in our experiments). Resonant transport (indicated by the black arrow) becomes possible when the levels (horizontal red bars) fall within the bias window, V (indicated by light orange shading). The Scheme illustrates resonant tunneling via an empty level, but such tunneling can also occur via an occupied level, below the Fermi level.

in current. Here, for the CytC(E104C), the C-heme/hemin cofactor lies approximately 1 nm away from the top AuNW electrode, embedded within its peptide matrix.[10] The importance of this geometry is that the cofactor is not exposed on the surface. As a result, the coupling between the C-heme/hemin cofactor and nearest Au electrode is weak, preserving the integrity of the C-heme/hemin cofactor electronic states when the protein becomes part of the junction. The weak interactions between the electrodes and the C-heme/hemin cofactor allows changing the energy levels of the latter with respect to the Fermi levels of the electrodes, i.e., Fermi level pinning is negligible. Therefore, sweeping the bias across the junction allows access to the electronic states within the Au–protein–Au system.

Conclusion

To summarize, we report a clear observation of conductance resonances in an intimate-contact solid-state protein junction (without any linker) by only varying the applied bias. Systematic study of the experimentally obtained conductance–voltage profiles for Au–CytC–Au junctions, suggest that one can switch the transport mechanism from on- to off-resonance by changing the bias between the electrodes. At less than 0.5 V bias, the charge-transport mechanism is consistent with off-resonant tunneling. Whereas, at greater than 0.5 V, we show that it is possible to sweep the bias window across the C-heme/hemin cofactor electronic states enabling resonant tunneling via Au–CytC–Au junctions. The ab initio DFT calculations carried out on the large data set of the whole structure of Cyt C(E104C) attached to the Au surface, further supports the involvement of the heme/hemin cofactor electronic states in the charge-transport process. Understanding and manipulating these features at the molecular level can lead us to the point where bio-electronic technologies can be realistically attained.

Experimental Section

The process of forming CytC(E104C) monolayers and junction fabrication is described in Section 1 of the Supporting Information. Briefly, μm-sized Au electrode pairs were fabricated on a Si wafer by photolithography. Monolayers of CytC(E104C) were prepared by using the surface-exposed cysteine 104 residue that binds covalently to the micro-fabricated Au electrode in such a way that its hemin is proximal to the top Au nanowire (AuNW) electrode (0.8–0.9 nm between the Fe^{III} ion and the physical top contact).[10] The Au-bound CytC mutant (E104C) yields oriented monolayers, sufficiently robust to carry out solid-state electron-transport measurements[19] at both room and cryogenic temperatures (approximately 10–15 K).[20] The protein monolayers were characterized by ellipsometry and atomic force microscopy (thickness), UV/Vis, and PM-IRRAS spectroscopies (Supporting Information, Figure S3). The "suspended-wire" technique[21,22] was used to form the top electrical contact, where individual Au nanowires were electrostatically trapped between two lithographically prepared Au electrodes, thereby forming a junction between the CytC(E104C) monolayer on one of the Au electrodes and the electrostatically trapped single Au nanowire.

Acknowledgements

J.F. is grateful to the Azrieli Foundation for the award of an Azrieli Fellowship. D.C. and M.S. thank the Israel Science Foundation, the Minerva Foundation (Munich), the Nancy and Stephen Grand Center for Sensors and Security, the Benoziyo Endowment Fund for the Advancement of Science, and the J & R Center for Scientific Research for partial support. M.S. holds the Katzir-Makineni Chair in Chemistry. C.R.M., J.C.C., and L.A.Z. were funded by the Spanish MINECO through the grants MAT2014-58982-JIN, MDM-2014-0377, and FIS2017-84057-P, respectively. D.A.D. and R.V.C. acknowledge financial support from the Russian Academy of Sciences program "Molecular and Cellular Biology". The authors thankfully acknowledge the computer resources, technical expertise, and assistance provided by the Red Española de Supercomputación (RES) at the Marenostrum supercomputer (BSC, Barcelona).

Conflict of interest

The authors declare no conflict of interest.

Keywords: bioelectronic junction · electron transfer · on–off switching · resonant tunneling

How to cite: *Angew. Chem. Int. Ed.* **2019**, *58*, 11852–11859
Angew. Chem. **2019**, *131*, 11978–11985

[1] C. D. Bostick, S. Mukhopadhyay, I. Pecht, M. Sheves, D. Cahen, D. Lederman, *Rep. Prog. Phys.* **2018**, *81*, 026601.
[2] A. Alessandrini, P. Facci, *Eur. Polym. J.* **2016**, *83*, 450–466.
[3] N. Amdursky, D. Marchak, L. Sepunaru, I. Pecht, M. Sheves, D. Cahen, *Adv. Mater.* **2014**, *26*, 7142–7161.
[4] "Electron transfer through proteins": J. R. Winkler, H. B. Gray, T. R. Prytkova, I. V. Kurnikov, D. N. Beratan, *Bioelectronics: From Theory to Applications*, Wiley, Hoboken, **2005**, pp. 15–33.
[5] I. Ron, L. Sepunaru, S. Itzhakov, T. Belenkova, N. Friedman, I. Pecht, M. Sheves, D. Cahen, *J. Am. Chem. Soc.* **2010**, *132*, 4131–4140.
[6] K. S. Kumar, R. R. Pasula, S. Lim, C. A. Nijhuis, *Adv. Mater.* **2016**, *28*, 1824–1830.
[7] M. P. Ruiz, A. C. Aragonès, N. Camarero, J. G. Vilhena, M. Ortega, L. A. Zotti, R. Pérez, J. C. Cuevas, P. Gorostiza, I. Díez-Pérez, *J. Am. Chem. Soc.* **2017**, *139*, 15337–15346.
[8] Z. F. Liu, J. B. Neaton, *J. Phys. Chem. C* **2017**, *121*, 21136–21144.
[9] J. A. Fereiro, X. Yu, I. Pecht, M. Sheves, J. C. Cuevas, D. Cahen, *Proc. Natl. Acad. Sci. USA* **2018**, *115*, E4577–E4583.
[10] N. Amdursky, D. Ferber, C. A. Bortolotti, D. A. Dolgikh, R. V. Chertkova, I. Pecht, M. Sheves, D. Cahen, *Proc. Natl. Acad. Sci. USA* **2014**, *111*, 5556–5561.
[11] J. A. Fereiro, G. Porat, T. Bendikov, I. Pecht, M. Sheves, D. Cahen, *J. Am. Chem. Soc.* **2018**, *140*, 13317–13326.
[12] B. Kayser, J. A. Fereiro, C. Guo, S. R. Cohen, M. Sheves, I. Pecht, D. Cahen, *Nanoscale* **2018**, *10*, 21712–21720.
[13] S. Y. Sayed, J. A. Fereiro, H. J. Yan, R. L. McCreery, A. J. Bergren, *Proc. Natl. Acad. Sci. USA* **2012**, *109*, 11498–11503.
[14] Q. J. Chi, O. Farver, J. Ulstrup, *Proc. Natl. Acad. Sci. USA* **2005**, *102*, 16203–16208.

[15] V. Frascerra, F. Calabi, G. Maruccio, P. P. Pornpa, R. Cingolani, R. Rinaldi, *IEEE Trans. Nanotechnol.* **2005**, *4*, 637 – 640.
[16] P. Facci, D. Alliata, S. Cannistraro, *Ultramicroscopy* **2001**, *89*, 291 – 298.
[17] Z. T. Xie, I. Baldea, C. E. Smith, Y. F. Wu, C. D. Frisbie, *ACS Nano* **2015**, *9*, 8022 – 8036.
[18] I. Bertini, G. Cavallaro, A. Rosato, *Chem. Rev.* **2006**, *106*, 90 – 115.
[19] C. Baldacchini, A. R. Bizzarri, S. Cannistraro, *Eur. Polym. J.* **2016**, *83*, 407 – 427.
[20] X. Yu, R. Lovrincic, L. Sepunaru, W. Li, A. Vilan, I. Pecht, M. Sheves, D. Cahen, *ACS Nano* **2015**, *9*, 9955 – 9963.
[21] P. A. Smith, C. D. Nordquist, T. N. Jackson, T. S. Mayer, B. R. Martin, J. Mbindyo, T. E. Mallouk, *Appl. Phys. Lett.* **2000**, *77*, 1399 – 1401.
[22] E. M. Freer, O. Grachev, X. F. Duan, S. Martin, D. P. Stumbo, *Nat. Nanotechnol.* **2010**, *5*, 525 – 530.
[23] M. Araidai, M. Tsukada, *Phys. Rev. B* **2010**, *81*, 235114.
[24] I. Bâldea, *Phys. Rev. B* **2012**, *85*, 035442.
[25] J. C. Cuevas, E. Scheer, *Molecular electronics: An introduction to theory and experiment*, *Vol. 15*, World Scientific, London, **2017**.
[26] T. Ozaki, *Phys. Rev. B* **2003**, *67*, 155108.
[27] T. Ozaki, H. Kino, *Phys. Rev. B* **2004**, *69*, 195113.
[28] C. Romero-Muñiz, M. Ortega, J. G. Vilhena, I. Díez-Pérez, J. C. Cuevas, R. Pérez, L. A. Zotti, *Phys. Chem. Chem. Phys.* **2018**, *20*, 30392 – 30402.
[29] N. Amdursky, D. Ferber, I. Pecht, M. Sheves, D. Cahen, *Phys. Chem. Chem. Phys.* **2013**, *15*, 17142 – 17149.
[30] N. S. Wigginton, K. M. Rosso, M. F. Hochella, *J. Phys. Chem. B* **2007**, *111*, 12857 – 12864.
[31] A. Vilan, *Phys. Chem. Chem. Phys.* **2017**, *19*, 27166 – 27172.

Manuscript received: May 15, 2019
Accepted manuscript online: June 27, 2019
Version of record online: July 25, 2019

